AGU PUBLICATIONS

Radio Science

RESEARCH ARTICLE
10.1002/2015RS005874

A novel band-pass filter based on a periodically drilled SIW structure

A. Coves[1], G. Torregrosa-Penalva[1], A. A. San-Blas[1], M. A. Sánchez-Soriano[2], A. Martellosio[3], E. Bronchalo[1], and M. Bozzi[3]

[1]Departamento de Ingeniería de Comunicaciones, Universidad Miguel Hernández de Elche, Elche, Spain, [2]Departamento de Física, Ing. de Sistemas y Teoría de la Señal, Instituto de Física Aplicada a las Ciencias y Tecnologías, Universidad de Alicante, Alicante, Spain, [3]Department of Electrical, Computer and Biomedical Engineering, University of Pavia, Pavia, Italy

Key Points:
- A band-pass filter is demonstrated using high- and low-impedance SIW sections
- A lower permittivity can be achieved by performing arrays of air holes along the waveguide
- A prototype of the designed filter has been fabricated and measured, showing a good agreement between measurements and simulations

Correspondence to:
A. Coves,
angela.coves@umh.es

Citation:
Coves, A., G. Torregrosa-Penalva, A. A. San-Blas, M. A. Sánchez-Soriano, A. Martellosio, E. Bronchalo, and M. Bozzi (2016), A novel band-pass filter based on a periodically drilled SIW structure, *Radio Sci.*, *51*, 328–336, doi:10.1002/2015RS005874.

Received 25 NOV 2015
Accepted 19 MAR 2016
Accepted article online 25 MAR 2016
Published online 25 APR 2016

Abstract The design and fabrication of a band-pass step impedance filter based on high and low dielectric constant sections has been realized on substrate integrated waveguide (SIW) technology. The overall process includes the design of the ideal band-pass prototype filter, where the implementation of the impedance inverters has been carried out by means of waveguide sections of lower permittivity. This can be practically achieved by implementing arrays of air holes along the waveguide. Several SIW structures with and without arrays of air holes have been simulated and fabricated in order to experimentally evaluate their relative permittivity. Additionally, the equivalent filter in SIW technology has been designed and optimized. Finally, a prototype of the designed filter has been fabricated and measured, showing a good agreement between measurements and simulations, which demonstrates the validity of the proposed design approach.

1. Introduction

In recent years, many papers have been published on a new type of transmission line called substrate integrated waveguide (SIW) [*Deslandes and Wu*, 2001; *Cassivi et al.*, 2002]. This low-cost realization of the traditional rectangular waveguide takes the advantages of planar lines for easy integration with other circuits and of waveguides for low radiation losses [*Chen and Wu*, 2014a]. This technology is indicated for implementing devices working at frequencies where lumped elements, or even its distributed microstrip circuit counterparts, present parasitic effects and high losses, which make them unpractical. It is then possible to implement waveguide components and planar circuits using the same process without any additional step. Filters, which are key devices in many communication systems [*Rostami and Rostami*, 2004; *Engheta et al.*, 2005; *Valagiannopoulos*, 2011a; *Alù and Engheta*, 2006; *Sun et al.*, 2012; *Valagiannopoulos*, 2008], are an example of microwave circuits that can be realized in SIW technology. There are many techniques to achieve filtering behavior in SIW structures. Some techniques, such as using inductive diaphragms, cavity filters or periodic metallic posts along the conventional rectangular waveguides [*Chen and Wu*, 2014b], defected ground structures, or embedded resonators [*Farzami and Norooziarab*, 2013; *Dong et al.*, 2009; *Norooziarab et al.*, 2012], have been implemented in SIW technology to develop filtering responses. Furthermore, stepped impedance waveguide filters can be realized by loading the SIW structure with periodically different dielectric sections [*Solano et al.*, 2005].

In this work, the use of the latter technique is proposed for the design and practical implementation of a waveguide microwave filter based on the combination of different permittivity SIW sections. The synthesis of a lower effective permittivity region in a SIW can be achieved by adding arrays of air holes along the waveguide [*Isidro et al.*, 2013]. The effect of the geometry of the air holes on the effective permittivity has been numerically studied using the commercial software tool Ansys High Frequency Structural Simulator (HFSS). This study provides an optimum number of air holes (and their diameters), for the width of the particular waveguide under study, which minimizes the waveguide effective permittivity. This study also shows that the shielding of the drilled waveguide leads to a reduction of its effective permittivity. The results of this study have been used for the design of a new topology of band-pass filter in SIW technology based on stepped impedance filters. The inclusion of air holes in some regions of the filter in order to lower their relative permittivity leads to a decrease of the dielectric losses due to the removal of substrate material and provides a spurious free range similar to those of traditional filters using metallic irises [*Coves et al.*, 2015]. For validation purposes, several sections of standard and drilled SIWs of different lengths have been both simulated and measured, and the

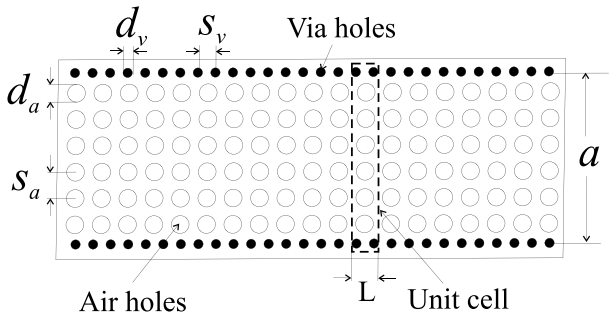

Figure 1. Scheme of a SIW with periodic air holes.

corresponding dispersion curves have been successfully compared. Finally, a prototype of the designed filter has been fabricated and measured, showing a good agreement between measurements and simulations, which demonstrates the validity of the proposed topology.

2. Study of the Effective Permittivity of a SIW With Periodic Air Holes

Figure 1 shows the scheme of a section of the waveguide under study, consisting of a conventional SIW in which several arrays of air holes are added along the waveguide, in this case following a rectangular pattern. The air holes are characterized by their separation s_a and diameter d_a. This waveguide is formed by two rows of parallel metallic posts (or via holes) delimiting the area of propagation of the fundamental TE_{10} mode of the SIW. The metallic posts are characterized by their separation s_v and diameter d_v. Their values must be appropriately chosen [*Deslandes and Wu*, 2001] in order to avoid radiation losses, so they must fulfill the following conditions:

$$d_v < \lambda_g/5, \quad s_v \leq 2d_v \tag{1}$$

where λ_g is the guided wavelength. The propagation constant of this guide is determined by the width a of the SIW (see Figure 1) and also by the effective permittivity ϵ_{reff} obtained after making the air holes in the propagation area in order to reduce the waveguide effective permittivity. Moreover, a decrease of the dielectric losses is expected due to the removal of material, which is an interesting feature in filter design. A previous study [*Cassivi et al.*, 2002] demonstrates that a SIW can be analyzed as an equivalent rectangular waveguide of effective width a_{eff} given by

$$a_{eff} = a - \frac{d_v^2}{0,95 s_v} \tag{2}$$

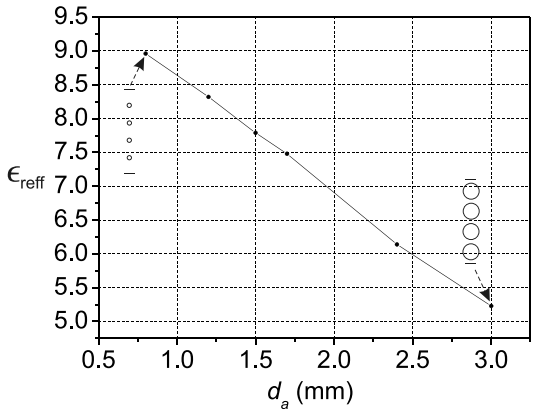

Figure 2. Effective relative permittivity ϵ_{reff} given by equation (3) obtained when four air holes are drilled equally spaced across the width of the guide, for different diameters of the air holes.

Therefore, all the study performed in this section is carried out using the equivalent waveguide of width a_{eff} given by equation (2) and height b. It is worth mentioning that it has been checked by numerical simulation [*Isidro et al.*, 2013] that when the drilled guide is not shielded in the top and bottom walls, the electric field is mainly confined in the dielectric material, so that ϵ_{reff} is close to the substrate permittivity. However, for the shielded waveguide, the electric field distributes transversely through the air holes following the TE_{10} mode profile, which implies a considerable reduction of its effective permittivity. Consequently, a 20 μm thick copper layer has been placed on the top and bottom layers of the drilled waveguide, with the purpose of shielding the structure and thus avoiding the electric field to overlap the air holes.

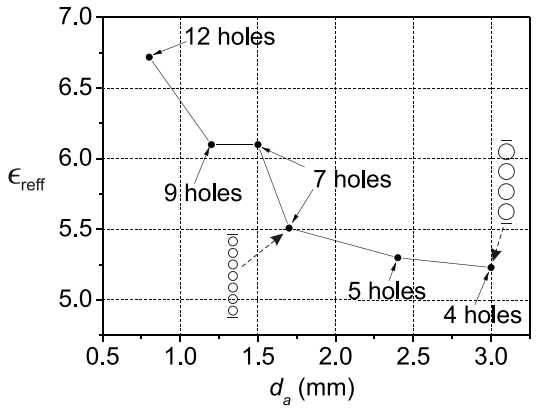

Figure 3. Effective relative permittivity ϵ_{reff} given by equation (3) obtained when a different number of air holes are drilled equally spaced across the width of the guide, with different diameters.

In order to accurately obtain the effective permittivity of a drilled waveguide, the commercial software tool Ansys HFSS has been employed. The eigenmode module of such analysis tool yields the cutoff frequencies of the waveguide modes. In this case, we have restricted our study to the monomode regime of the waveguide, so that it is possible to relate the effective permittivity of the waveguide with the cutoff frequency of the TE_{10} mode through the following expression:

$$\epsilon_{reff} = \frac{c^2}{4a_{eff}^2 f_c^2} \tag{3}$$

where c is the speed of light in free space and f_c is the cutoff frequency of the first waveguide mode provided by the software simulation. For each air hole pattern analyzed, given that periodic conditions are met along the waveguide, we only need to analyze a periodic unit cell along the direction of propagation (see Figure 1). Thus, in the rectangular pattern case, we have analyzed a periodic cell of dimensions $a_{eff} \times b$ and length $L = d_a + 0.25$ mm, being d_a the hole diameter and 0.25 mm the minimum distance between air holes in order to guarantee a certain mechanical strength. Using equation (3), we have obtained the effective relative permittivity of a waveguide of dimensions $a_{eff} = 15.8$ mm (with a cutoff frequency $f_c = 3$ GHz in the absence of air holes), and $b = 0.63$ mm (corresponding to the height of the substrate employed—Taconic CER-10— with $\epsilon_r = 10$), in which a periodic array of air holes have been periodically made.

2.1. Analysis of a Fixed Number of Air Holes in the Unit Cell

A first analysis has been performed varying d_a (delimited by the availability of drills in the manufacturing process), for a fixed number of four air holes in the unit cell. In Figure 2 it is represented the effective relative permittivity ϵ_{reff} given by equation (3) obtained for different diameters of the air holes equally spaced across the width of the guide see the insets in Figure 2). From this figure, it can be deduced that the increase of the hole size makes the value of the effective relative permittivity to decrease, due to the reduction in the dielectric volume ratio.

2.2. Analysis of a Maximum Number of Air Holes in the Unit Cell

A second analysis has been performed where the maximum number of air holes equally spaced across the width of the guide is used. This number depends on the diameter of the air holes (see the insets in Figure 3). The objective of this second analysis is to maximize the area occupied by the air holes in the unit cell.

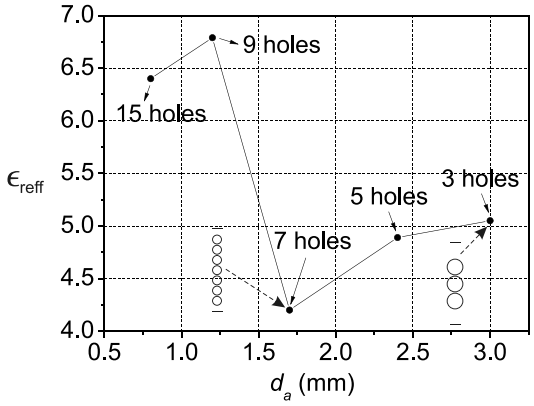

Figure 4. Effective relative permittivity ϵ_{reff} given by equation (3) obtained when an odd number of air holes are drilled across the width of the guide, starting from the center of the guide and are distant from each other a minimum constant distance of 0.25 mm.

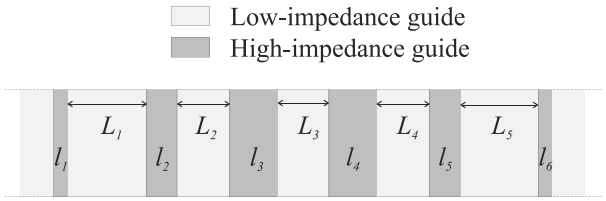

Figure 5. Top view of a fifth-order step-impedance rectangular filter.

In this case, when comparing these results to those of section 2.1, a much lower value of the effective relative permittivity is achieved for a particular air hole diameter. It is then evident that in order to minimize the effective relative permittivity, it is necessary to maximize the volume occupied by air holes. However, knowing the fundamental mode TE_{10} electric field distribution in the guide, it would be more efficient to remove most of the dielectric in the central part of the guide where the electric field is more intense.

2.3. Analysis of a Maximum Number of Air Holes Centered in the Unit Cell for a Minimum Hole Spacing

Considering the previous results, a third analysis has been performed where the air holes have been placed starting from the center of the guide and are spaced 0.25 mm (minimum distance to ensure a certain mechanical strength)—see the insets in Figure 4— thus removing the dielectric material starting from the center of the guide. Figure 4 represents the dependence of the effective relative permittivity ϵ_{reff} with the diameter of odd numbers of air holes. An optimum configuration in this guide of seven air holes of diameter $d_a = 1.7$ mm provides the minimum value of $\epsilon_{reff} = 4.2$.

Thus, for this guide width, these analyses can be employed as a way of determining the drill diameter and the air hole positions for obtaining a desired value of ϵ_{reff}. In these studies it can be checked that ϵ_{reff} not always decreases when increasing the radius of the air holes. This fact is more evident when the air holes are placed starting from the center of the guide, which represents a higher inhomogeneity in the guide. Going a step farther, a rectangular volume of substrate material may have been removed from the center of the guide since the structure is shielded, but the mechanical strength of the filter diminishes dramatically, and it easily breaks during the fabrication process.

3. Design of a Band-Pass Waveguide-Based Microwave Filter Using Periodically Drilled SIW Technology

Next, we have applied the results of the previous section to the design of a five-pole Chebyshev filter, consisting of several sections of low-impedance rectangular waveguide (corresponding to the homogeneous high-permittivity dielectric filled waveguide) coupled with high-impedance sections (implemented by means of perforated sections with lower ϵ_{reff}), as shown in Figure 5. Although the filter design has been made in rectangular waveguide, the ultimate goal of this work is to implement the designed filter in SIW technology.

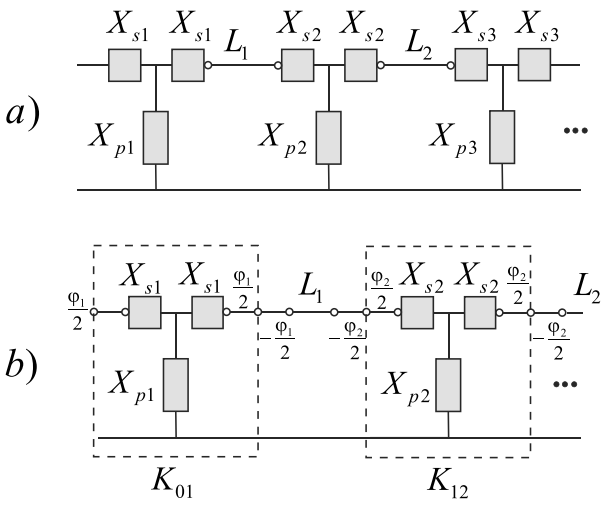

Figure 6. (a) Equivalent circuit model of a high-impedance waveguide section through a *T* network. (b) Equivalent impedance inverters model of a high-impedance waveguide section through a *T* network.

For the design of the waveguide-based filter, we have employed the *T* network equivalent circuit model of a high-impedance section [*Cameron et al.*, 2007], as shown in Figure 6a. The filter consists of half-wave resonators separated by high-impedance sections. Each high-impedance section is represented by two series reactances denoted by X_s and a shunt reactance denoted by X_p.

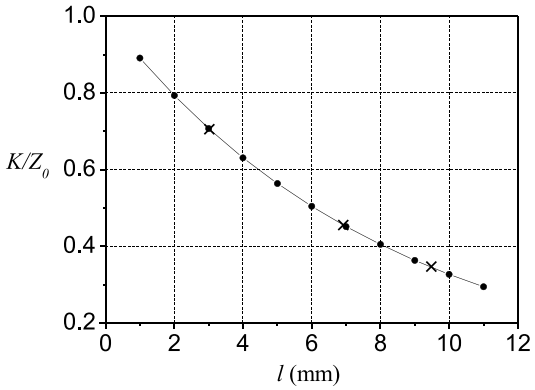

Figure 7. Impedance inverter factor K/Z_0 as a function of the high-impedance (drilled) rectangular waveguide length (l).

In order to transform it into the impedance inverters model, we use the impedance inverter circuit shown in Figure 6b, consisting of an inductive T network and two sections of length $\varphi/2$ on each side. The inverter is created by adding a length $\varphi/2$ and $-\varphi/2$ on each side of the discontinuity. In this case, the resonators are transmission lines of lengths L_n connected to two transmission lines of artificial lengths $-\varphi_n/2$ and $-\varphi_{n+1}/2$.

The specifications of the designed filter are the following: fifth-order band-pass Chebyshev filter with a center frequency $f_0 = 4$ GHz, a bandwidth of 600 MHz, and return loss of 15 dB. The rectangular waveguide has a width of $a_{\text{eff}} = 15.8$ mm and a height of $b = 0.63$ mm, corresponding to the thickness $b = h$ of the employed substrate, which in our case is a Taconic CER-10 substrate with $\epsilon_r = 10$ and $\tan\delta = 0.0035$ (http://www.taconic-add.com), double-sided metallized with a copper film 20 μm thick. Using the results provided in the previous analyses, high-impedance sections are implemented in all cases through drilled waveguides with air holes of diameter $d_a = 1.7$ mm spaced from each other a constant distance of 0.25 mm starting from the center of the guide, which provides the minimum value of $\epsilon_{\text{reff}} = 4.2$.

The coefficients of a fifth-order Chebyshev low-pass filter with $RL = 15$ dB are as follows: $g_0 = 1$, $g_1 = g_5 = 1.1468$, $g_2 = g_4 = 1.3712$, and $g_3 = 1.9750$. The center frequency of the filter and band-edge frequencies are related by

$$f_0 = \sqrt{f_1 f_2}, \quad \text{BW} = f_1 - f_2, \tag{4}$$

which give $f_1 = 3.7$ GHz, $f_2 = 4.3$ GHz. The filter relative bandwidth is

$$\Delta = \frac{\lambda_{g1} - \lambda_{g2}}{\lambda_{g0}} = 0.3636 \tag{5}$$

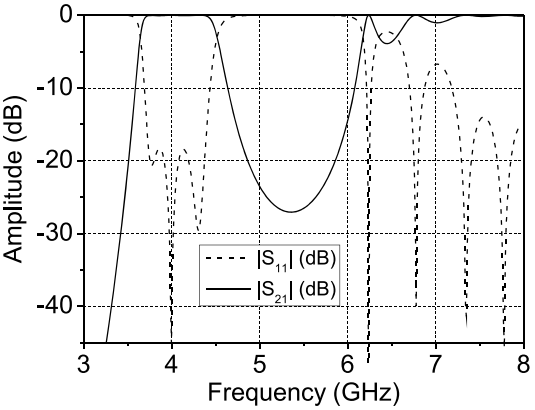

Figure 8. Electrical response of the designed step-impedance rectangular waveguide filter.

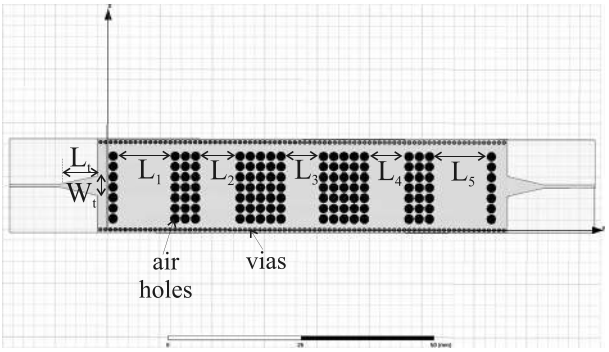

Figure 9. Scheme of the designed filter in SIW technology.

Then, the values obtained for the impedance inverter factors are [*Cameron et al.*, 2007] as follows:

$$\frac{K_{01}}{Z_0} = \frac{K_{56}}{Z_0} = \sqrt{\frac{\pi\Delta}{2g_0g_1}} = 0.7051 \tag{6}$$

$$\frac{K_{12}}{Z_0} = \frac{K_{45}}{Z_0} = \frac{\pi\Delta}{2\sqrt{g_1g_2}} = 0.45546 \tag{7}$$

$$\frac{K_{23}}{Z_0} = \frac{K_{34}}{Z_0} = \frac{\pi\Delta}{2\sqrt{g_2g_3}} = 0.34706 \tag{8}$$

where $Z_0 = 50\ \Omega$ is the reference impedance of the input and output ports.

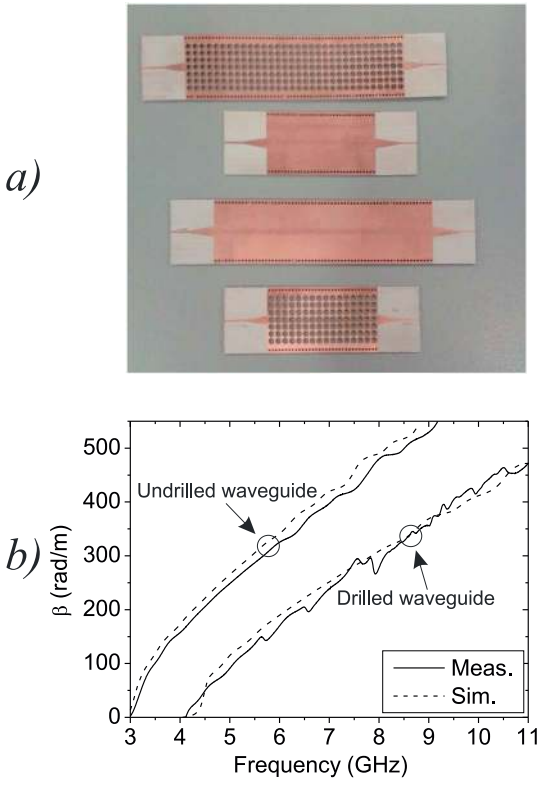

Figure 10. (a) Photograph of several sections of fabricated SIWs. (b) Comparison of simulated and measured dispersion curves of the fabricated SIWs.

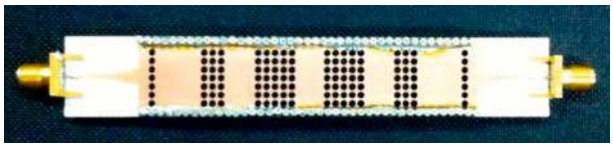

Figure 11. Photograph of the fabricated step-impedance filter.

The scattering parameters of a high-impedance section (referred to the dielectric discontinuity planes), assuming that it is homogeneously filled with a dielectric material of relative permittivity ϵ_{reff}, can be analytically obtained, which are related to the T network elements shown in Figure 6a, X_s and X_p, by the following equations [*Cameron et al.*, 2007]:

$$j\frac{X_s}{Z_0} = \frac{1 - S_{12} + S_{11}}{1 - S_{11} + S_{12}} \tag{9}$$

$$j\frac{X_p}{Z_0} = \frac{2S_{12}}{\left(1 - S_{11}\right)^2 - S_{12}^2} \tag{10}$$

where S_{11}, S_{21}, and S_{12} are the scattering parameters related to the TE_{10} fundamental mode of the input (low-impedance) waveguide at the center frequency of the filter, f_0. For the impedance inverter shown in Figure 6b, X_s and X_p are related to K/Z_0 and φ by

$$\frac{K}{Z_0} = \left|\tan\left(\frac{\varphi}{2}\arctan\frac{X_s}{Z_0}\right)\right| \tag{11}$$

$$\varphi = -\arctan\left(2\frac{X_p}{Z_0} + \frac{X_s}{Z_0}\right) - \arctan\frac{X_s}{Z_0} \tag{12}$$

and thus, the resonator lengths are given by the following equation:

$$L_n = \frac{\lambda_{g0}}{2\pi}\left[\pi + \frac{1}{2}\left(\varphi_n + \varphi_{n+1}\right)\right], \quad n = 1, \ldots, N \tag{13}$$

The scattering parameters of several high-impedance waveguide sections of different lengths have been obtained, ranging from 1 to 11 mm, providing the curve shown in Figure 7 where the impedance inverter factor K/Z_0 is represented with dots as a function of the high-impedance waveguide section length l. From the curve represented in Figure 7 and the values of the inverter factors provided by equations (6)–(8), the following values of the high-impedance rectangular waveguide lengths have been deduced for our filter: $l_1 = l_6 = 3.02$ mm, $l_2 = l_5 = 6.92$ mm, and $l_3 = l_4 = 9.48$ mm. For these values of high-impedance waveguide lengths, the obtained phases given by equation (12) yield the following values of the resonator lengths: $L_1 = L_5 = 7.52$ mm, $L_2 = L_4 = 6.83$ mm, and $L_3 = 6.63$ mm. In Figure 8 we have represented the S parameters of the designed step-impedance waveguide filter computed by its equivalent circuit. In the simulation, we have used the $Z_{TE_{10}}$ impedances for low ($\epsilon_r = 10$) and high ($\epsilon_{reff} = 4.2$) impedance waveguide sections of different lengths L_i and l_i. Thus, the results represented in Figure 8 have been easily computed without solving the whole structure with a full-wave software and without including the effect of conductor and dielectric losses. In this figure, it can be seen that the designed filter meets the design specifications.

Once the different waveguide sections of high and low impedance have been obtained, the next step in the design process is to determine the number of air hole rows in the high-impedance sections, the equivalent rectangular width a in SIW technology, and the design of the microstrip to SIW transition. To this aim, the following parameters for the via holes have been employed: $d_v = 0.7$ mm and $s_v = 0.95$ mm. With the equivalence given by equation (2), the width of the different sections of SIWs is $a = 16.34$ mm. On the other hand, for the microstrip to SIW transition, the same transition presented in *Deslandes and Wu* [2001] has been implemented, consisting of a microstrip taper (see Figure 9). These transitions provide a wide bandwidth and can be designed to cover the entire operation band of the proposed filter. Finally, an optimization process of

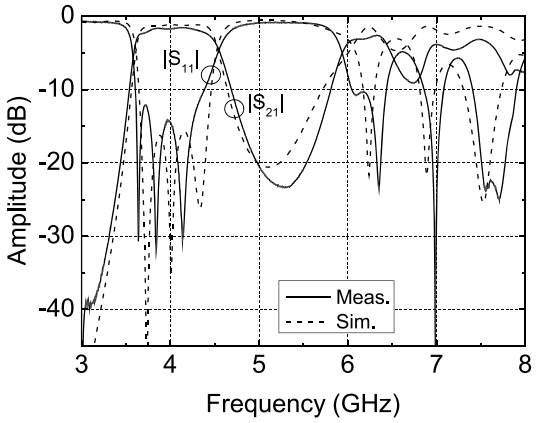

Figure 12. Simulated and measured response of the designed filter in SIW technology.

the designed filter response has been performed with Ansys HFSS, providing the following final filter parameters: $L_1 = L_5 = 10.12$ mm, $L_2 = L_4 = 6.79$ mm, and $L_3 = 6.42$ mm. The dimensions of the taper transition are $W_t = 3.74$ mm and $L_t = 7.37$ mm, respectively, while the width of the microstrip line is of 0.6 mm ($Z_0 = 50\,\Omega$). The lengths L_1 and L_5 of the final optimized prototype differ from the initial design values due to the effect of the microstrip to SIW transition. In Figure 9 it is represented a scheme of the designed SIW filter with its final dimensions.

4. Fabrication and Experimental Results

Several drilled and undrilled SIW sections including microstrip to SIW transitions have been designed and fabricated (see Figure 10a) in order to experimentally obtain their relative permittivity. The manufacturing process is divided in three steps. First of all, an LPKF prototyping machine is used to drill the holes and mill the planar circuits. Second, the metallic vias are added to form the waveguide sidewalls. Finally, a thin layer of copper is soldered over the air holes on the top and bottom sides of the substrate.

For each type of SIW (drilled and undrilled), the propagation constant can be evaluated from the scattering parameters obtained for two different lengths using the same approach as that presented in [*Deslandes and Wu*, 2001]. The simulated and measured dispersion curves of the two types of SIWs are presented in Figure 10b, showing a good agreement in all the represented operation band. These results show that an air-drilled SIW section behaves as a conventional SIW with a relative effecitive permittiviy given by equation (3). Other approaches, such as the ones reported in *Valagiannopoulos and Uzunoglu* [2007] and *Valagiannopoulos* [2011b], may be also employed in order to study the propagation characteristics of the air-drilled SIW sections.

On the other hand, a photograph of the fabricated filter is shown in Figure 11 (before soldering the copper layer over the air holes). The simulated response of the designed filter in SIW technology is shown in Figure 12 with dashed line, including the effect of conductor and dielectric losses. In this figure it is also represented, with solid line, the measured response of the filter, exhibiting a good agreement between the simulated and measured responses. The measured response shows a good impedance matching in the passband (better than 12 dB) and low insertion losses (1.6 dB in the center of the passband) and also a good out of band rejection performance (better than 20 dB).

5. Conclusion

A practical design example of a waveguide step-impedance filter using the impedance inverter model is shown, using SIW sections of high and low impedance as a low cost and easy to manufacture technology. A systematic study demonstrates that high-impedance sections can be practically achieved by performing arrays of air holes along the waveguide in order to synthesize a lower effective permittivity. An example of a band-pass filter centered at 4 GHz has been designed, optimized, and fabricated to show the whole design and fabrication process, showing a good agreement between measurements and simulations.

Acknowledgments
All the data necessary to understand, evaluate, replicate, and generate the figures and results presented in this paper have been included in the present manuscript. The commercial software Ansys HFSS has been used to generate the simulated results provided by the authors. This work was supported by the Ministerio de Economía y Competitividad, Spanish Government, under the Research Project TEC2013-47037-C5-4-R.

References

Alù, A., and N. Engheta (2006), Optical nanotransmission lines: Synthesis of planar left-handed metamaterials in the infrared and visible regimes, *J. Opt. Soc. Am. B Opt. Phys.*, *23*, 571–583.

Cameron, R. J., C. M. Kudsia, and R. R. Mansour (2007), *Microwave Filters for Communication Systems: Fundamentals, Design and Applications*, Wiley, Chichester, England.

Cassivi, Y., L. Perregrini, P. Arcioni, M. Bressan, K. Wu, and G. Conciauro (2002), Dispersion characteristics of substrate integrated rectangular waveguide, *IEEE Microwave Wireless Compon. Lett.*, *12*(9), 333–335.

Chen, X. P., and K. Wu (2014a), Substrate integrated waveguide filters: Practical aspects and design considerations, *IEEE Microwave Mag.*, *15*(7), 75–83.

Chen, X. P., and K. Wu (2014b), Substrate integrated waveguide filters: Design techniques and structure innovations, *IEEE Microwave Mag.*, *15*(6), 121–133.

Coves, Á., Á. A. San Blas, S. Marini, G. Torregrosa, E. Bronchalo, and A. Martellosio (2015), Low-cost implementation of a waveguide-based microwave filter in substrate integrated waveguide (SIW) technology, paper presented at 2015 PIERS Proc., pp. 537–541, Prague, Czech Republic, 6–9 Jul.

Deslandes, D., and K. Wu (2001), Integrated microstrip and rectangular waveguide in planar form, *IEEE Microwave Wireless Compon. Lett.*, *11*(2), 68–70.

Dong, Y. D., T. Yang, and T. Itoh (2009), Substrate integrated waveguide loaded by complementary split-ring resonators and its applications to miniaturized waveguide filters, *IEEE Trans. Microwave Theory Tech.*, *57*(9), 2211–2223.

Engheta, N., A. Salandrino, and A. Alù (2005), Circuit elements at optical frequencies: Nanoinductors, nanocapacitors, and nanoresistorss, *Phys. Rev. Lett.*, *95*, 095504.

Farzami, F., and M. Norooziarab (2013), Experimental realization of tunable transmission lines based on single-layer SIWs loaded by embedded SRRs, *IEEE Trans. Microwave Theory Tech.*, *61*(8), 2848–2857.

Isidro, R., Á. Coves, M. A. Sánchez-Soriano, G. Torregrosa, E. Bronchalo, and M. Bozzi (2013), Systematic study of the effective permittitivy in a periodically drilled substrate integrated waveguide, paper presented at 2013 PIERS Proc., pp. 1870–1874, Stockholm, Sweden, 12–15 Aug.

Norooziarab, M., M. Rafaei-Booket, Z. Atlasbaf, and F. Farzami (2012), A tunable transmission line based on an SIW loaded by a new single-cell metamaterial, paper presented at 6th International Symposium on Telecommunications (IST), pp. 75–79.

Rostami, A., and G. Rostami (2004), Full-optical realization of tunable low pass, high pass and band pass optical filters using ring resonators, *Opt. Commun.*, *240*(1–3), 133–151.

Sun, Y., B. Edwards, A. Alù, and N. Engheta (2012), Experimental realization of optical lumped nanocircuits at infrared wavelengths, *Nat. Mater.*, *11*, 208–211.

Solano, M. A., A. Gómez, A. Lakhtakia, and A. Vegas (2005), Rigorous analysis of guided wave propagation of dielectric electromagnetic band-gaps in a rectangular waveguide, *Int. J. Electron.*, *92*(2), 117–130.

Valagiannopoulos, C. A. (2008), On examining the influence of a thin dielectric strip posed across the diameter of a penetrable radiating cylinder, *Progr. Electromagn. Res.*, *3*, 203–214.

Valagiannopoulos, C. A. (2011a), Electromagnetic propagation into parallel-plate waveguide in the presence of a skew metallic surface, *Electromagnetics*, *31*(8), 593–605.

Valagiannopoulos, C. A. (2011b), Electromagnetic scattering of the field of a metamaterial slab antenna by an arbitrarily positioned cluster of metallic cylinders, *Progr. Electromagn. Res.*, *114*, 51–66.

Valagiannopoulos, C. A., and N. K. Uzunoglu (2007), Rigorous analysis of a metallic circular post in a rectangular waveguide with step discontinuity of sidewalls, *IEEE Trans. Microwave Theory Tech.*, *55*(8), 1673–1684.